

# Numerical sensitivity analysis of graded superlattice quantum cascade laser structures

David Z.-Y. Ting, Martin G. Young

D. Z.-Y. Ting and M. G. Young are with the Center for Space Microelectronics Technologies, Jet Propulsion Laboratory, California Institute of Technology, Pasadena, CA 91109 USA

The work described in this paper was performed by the Center for Space Microelectronics Technology, Jet Propulsion Laboratory, California Institute of Technology under contract with the National Aeronautic and Space Administration.

### Abstract

We use a two-band tight-binding model to analyze the basic electronic, optical, and transmission properties of the graded superlattice quantum cascade laser (QCL) design. We prescribe a simple procedure for estimating the bounds of the operating voltage range of a QCL. We also conduct a series of numerical sensitivity analyses in which we systematically introduce small changes to the design of a reference graded superlattice QCL. We find that uniform scaling of layer widths of up to approximately  $\pm 5\%$  would not significantly affect laser performance. However, uniform scaling results in shifts in lasing wavelength, and this effect can be exploited for fine tuning the lasing wavelength with only minimal effort in redesign. We examine the effect of random layer width variations and found rather large effects on QCL properties. The fact that QCL properties seem to be more sensitive to random layer width variations than systematic layer width variations (uniform scaling) underscores the importance of having an accurate design. Finally, we find that QCL designs seem to be fairly tolerant of interface grading, suggesting the possibility for less stringent growth requirement.

### Keywords

quantum cascade laser, modeling

## I. INTRODUCTION

The quantum cascade laser (QCL)[1] is a unipolar, semiconductor light source based on intersubband transitions. QCLs emitting in the 4 to 17  $\mu m$  range have been demonstrated[2], [3], [4], [5], [6], [7]. Since its introduction in 1994[1], the QCL has seen several design improvements.[8] The most recent design incorporates a graded superlattice as an active region, and has resulted in higher output power and lower threshold current density.[9] In this work, we analyze the graded superlattice QCL design theoretically. In particular, we perform numerical sensitivity analyses on selected design parameters to gain some understanding of the robustness of the design.

## II. METHOD

A number of simple band structure models can be used effectively to model intersubband devices.[10], [11], [12] In this work we use a two-band tight-binding model[13], [14] whose basis set consists of a linear chain of alternating  $s$  and  $p$  orbitals as illustrated in Fig. 1. The on-site energies are given by  $E_s = E_c$  and  $E_p = E_v$ , and the hopping matrix elements by  $t = [\hbar^2(E_s - E_p)/(2m^*d^2)]^{1/2}$  and  $u = t$  (in bulk), where  $E_c$  and  $E_v$  are

the conduction and valence band edges, respectively,  $m^*$  is the conduction band effective mass, and  $d$  is the distance between successive unit cells. The model may be considered as the tight-binding equivalent of the two-band  $k \cdot p$  model,[15] but with somewhat better computational efficiency and ease of implementation. Due to the absence of spurious evanescent states in the band gap, the simple transfer matrix method can be used for transmission coefficient calculations with minimal numerical instabilities.[14] Optical properties such as oscillator strengths can also be easily computed following the work of Kiledjian *et al.*[16] For applications to inter-conduction-subband devices, Nelson *et al.* obtained more accurate non-parabolicities by using an effective rather than the actual valence-band edge.[10] We apply the same procedure to the tight-binding model in this work. For modeling the lattice-matched InGaAs/InAlAs materials system, the following parameters are used:  $E_c(\text{InGaAs}) = 0$  eV,  $E_v(\text{InGaAs}) = -0.6816$  eV,  $m^*(\text{InGaAs}) = 0.043 m_0$ ,  $E_c(\text{InAlAs}) = 0.52$  eV,  $E_v(\text{InAlAs}) = -0.801$  eV, and  $m^*(\text{InAlAs}) = 0.078 m_0$ . [17]

### III. RESULTS

In this section we first use the two-band tight-binding model to analyze a reference graded superlattice QCL structure. We show how a simple set of criteria can be used to estimate the operating voltage range for a QCL. We then proceed to apply various perturbations to the reference structure for sensitivity analysis. We use the graded superlattice QCL published by Tredicucci and co-workers[9] as our reference device structure. Each cascading stage of this structure is 667 Å wide, and consists of a graded superlattice active region followed by an injector/Bragg reflector region. Fig.2 shows the zero-bias band diagram, energy levels, and probability densities for a single stage of the graded superlattice. To avoid clutter, only the dominant component (the s-component) of the probability density is shown for each state. It is evident from the figure that the states can be divided into distinct groups. We classify them according to whether their wave functions are localized in the active superlattice (“ASL-”) or the injector (“Inj-”) region, and according to the number of wave function nodes in each quantum well (one node for “2” states, none for “1” states; ). Note that due to well-width chirping, the lower-energy states within each group are localized to the left of the higher-energy states; the implications of this for optical properties will be discussed later.

Proper biasing must be applied to the QCL structure for lasing to occur. Fig.3 schematically illustrates the alignment of the different groups of states under three representative biasing conditions. The structure is designed for the lasing transition to take place between the lowest ASL-2 state and the highest ASL-1 state (from here on referred to as upper and lower states, respectively). Fig.3(a) illustrates the alignment of the groups of states under zero bias. It is essentially a simplified drawing of Fig.2, but with the addition of the Inj-2 states. Under proper biasing condition, as illustrated in Fig.3(b), population inversion is facilitated by removing the carriers in ASL-1 by resonant tunneling injection through Inj-1 states into the next stage. At the same time, the mis-alignment between ASL-2 and Inj-2 keeps the upper state confined in the active superlattice region, and available for radiative recombination. If the applied bias is too low, as in Fig.3(a), the ASL-1 states are confined and population inversion can not be established. On the other hand, if the applied bias is too high, as in Fig.3(c), the upper state can escape via resonant tunneling through Inj-2 states, and thereby reduce the number of carriers available for radiative recombination. These criteria can be used to define an approximate operating voltage range for the device. We demonstrate this in Fig.4, which shows the energy levels as functions of applied bias (per single stage). Under bias, mixing can take place among states from different groups, as is evident from the many anti-crossings in the figure. Three important (anti-)crossing points are highlighted in the figure: (1) The voltage associated with the crossing between the lowest ASL-1 state and the lowest Inj-1 state may be considered a lower limit of the operating range since some of the ASL-1 states would be confined below this bias. (2) Alternatively, the voltage at the crossing between the highest ASL-1 state and the highest Inj-1 state can also be considered, since Inj-1 states can be found between the lasing levels below this point. We therefore take the higher of these two crossing points as the lower limit on operating voltage. (3) The voltage at the crossing between the lowest ASL-2 state and the lowest Inj-2 state is taken as the upper limit since beyond this point resonant tunneling escape of carriers in the upper state can occur. Using this simple procedure, we obtain an operating range of 8.7 V to 12.5 V for a 28 period QCL, which appears to be in good general agreement with published experimental results[9].

Fig.5 shows the band diagram and energy levels of the reference structure biased within

the operating range. The right panel shows transmission probabilities through the injector region. We note that the injector region acts as a low-pass filter, allowing transmission of the ASL-1 states, but blocking the upper state. In this case, the transmission coefficient for the upper state is less than  $2 \times 10^{-7}$ , indicating good confinement. The probability densities for upper and lower states are also shown. Comparing to the corresponding probabilities densities in the zero-bias case shown in Fig.2, the wave functions involved in the lasing transition are now more strongly overlapped. Fig.6 shows the oscillator strengths between the upper state and the ASL-1 states as functions of applied bias. The top panel shows a simple case where only the active superlattice portion is used in the calculation. Superlattice QCL designs[18] exploit that fact that inter-miniband oscillator strength is the strongest between the top of a miniband and the bottom of the next highest miniband[19]. In order to keep the superlattice region field-free under operating bias, external doping in the injection region is introduced to counterbalance the applied field[20]. The improved graded superlattice design does not rely on external doping, but uses instead a chirping in the superlattice period to compensate for the applied bias[9]. However, this introduces a strong bias dependence in the oscillator strengths (see top panel of Fig.6) which must be taken into consideration in the design. The bias dependence of the oscillator strength associated with the lasing transition ( $f_{7,6}$ ) can be understood by examining the wave functions of the upper and lower lasing levels in Figs.2 and 5. The oscillator strength is weak under zero-bias where the two wave functions are centered at opposite ends of the superlattice region (Fig.2). With increasing bias, the wave functions slide towards each other, resulting in increasing oscillator strength. Eventually, the two wave functions would slide past each other, resulting in a decrease in the oscillator strength. The bottom panel of Fig.6 shows the results for the more complex case where both the active superlattice and the injector are used in the calculation. Essentially the same trend is observed for the oscillator strength between the lowest ASL-2 state and the highest ASL-1 state. However, due to mixing among ASL-1 and Inj-1 states (see Fig.4), the oscillator strength can be split between two nearby transitions associated with states involved in a level crossing. In the operating voltage range, the oscillator strength for the lasing transition indeed exceeds those for transitions between the lowest ASL-2 state

and the lower ASL-1 states, indicating the soundness of this design. Near the high end of the operating voltage range, we are again confronted with two nearby transitions with comparable oscillator strengths as the result of level crossing.

We next perform a series of sensitivity analyses by systematically introducing small changes to the reference structure. We characterize the effects due to these perturbations using the same quantities discussed above. First, we examine the effect of uniform scaling, which might result from miscalibrated growth rates. Next we examine structures where the positions of the interfaces are randomly displaced from the those of the reference structure to test for robustness against design or growth error. Finally, we analyze the effect of interface grading.

Fig.7 plots the lasing wavelengths, upper state transmission probabilities, and lasing transition oscillator strengths as functions of applied bias for five structures whose layer widths differ only by a uniform scaling factor (0.9 to 1.1). All data sets are plotted from the lower to the upper operating voltage, so that the operating voltage range for each structure can be read off directly. All five structures show essentially the same bias dependence. They all exhibit some variations (0.3 to 1.5  $\mu\text{m}$ ) in lasing wavelength, generally increasing with applied bias as a result of bias-dependent level mixing. The upper level transmission probabilities increases with applied bias due to barrier lowering. Oscillator strength dependences on applied bias are as previously discussed in Fig.6. Uniform layer width increase produces the following trends: (1) lasing wavelength increases as a result of increase in well widths, (2) upper state transmission probability decreases due to barrier widening, and, (3) oscillator strengths show a general increasing trend, in general agreement with previous modeling results on intersubband transitions in quantum wells [12]. Thus, for example, while a small amount of layer width reduction would decrease the upper state confinement, it is compensated by an increase in the lasing transition oscillator strength. In general, our results indicate that a uniform scaling change of  $\pm 5\%$  would not significantly degrade the laser performance. A practical consequence is that we can take a working design, and fine tune the lasing wavelength by performing a simple linear scaling.

Fig.8 examines the effects of random variations in layer widths. A set of ten structures

are generated from the reference structure by randomly displacing the position of each of the interfaces in each structure by -1, 0, or 1 Å ( $|\Delta x| = 1$  Å), all with equal probability. Note that  $|\Delta x|$  is smaller than the width of a single monolayer (2.94 Å). The effects of this small random layer width variation produces an approximately 1  $\mu\text{m}$  variation in lasing wavelengths, an order of magnitude variation in the upper state transmission probability, and 30% variations in oscillator strengths. We also note that there is a considerable spread in the operating ranges among the structures. In general, we find that the QCL properties we looked at are quite sensitive to random layer widths variations, and numerical experiments using larger  $\Delta x$  values confirm this observation. Fig.9 shows the results for  $|\Delta x| = 3$  Å (displacement of -3, -2, ..., or 3 Å). We find significant deviations from the properties of the reference structure.

Finally we examine the consequences of having linearly graded interfaces. At each interface, rather than shifting abruptly from InGaAs to InAlAs (or vice versa), we grade linearly from one material to the other over a ramp of finite width. Structures with ramp widths of 6 Å and 10 Å are examined in this calculation. Note that these ramp widths are rather substantial compared to the layer widths, which can be as small as 11 Å. Fig.10 shows reductions of 7% and 24% in the voltage operating range span for the structures with ramp widths of 6 Å and 10 Å, respectively, compared to the reference structure. The upper state transmission probability shows some increase with ramping, due to the softening of the barriers, but the lasing wavelengths and the oscillator strengths seem to be only minimally affected by interface grading. The calculated QCL properties of the 6 Å ramp structures differ only slightly from those of the reference structure; and those for 10 Å ramp structure also do not show significant deviations. These result suggest that a certain amount of unintended interface grading can be tolerated.

#### IV. SUMMARY

We performed theoretical analysis of basic electronic, optical, and transmission properties of the graded superlattice quantum cascade laser design using a two-band tight-binding model. We describe a simple procedure for estimating the operating voltage range of a QCL. We also conduct a series of sensitivity analyses through numerical simulations which systematically introduce small changes to the design of a reference graded super-

lattice QCL. We find that uniform scaling of layer widths of a few percent would not significantly affect laser performance. Also, uniform scaling results in shifts in lasing wavelength. This can be used for fine tuning the lasing wavelength with only minimal redesigning effort. We examined the effect of random layer width variations and found rather large effects on QCL properties. The fact that QCL properties seem to be more sensitive to random layer width variations than systematic layer width variations (uniform scaling) underscores the importance of having a good design. Finally, we found that QCL designs seem to be fairly tolerant of interface grading, suggesting the possibility for less stringent interface sharpness growth requirement.

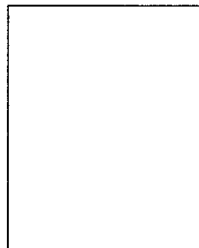
#### ACKNOWLEDGMENTS

The authors would like to acknowledge helpful discussion with S. Forouhar.

#### REFERENCES

- [1] J. Faist, F. Capasso, D.L. Sivco, C. Sirtori, A.L. Hutchinson, and A.Y. Cho, "Quantum cascade laser," *Science*, vol. 264, no. 5158, pp. 553–556, 1994.
- [2] J. Faist, F. Capasso, D.L. Sivco, A.L. Hutchinson, S.N.G. Chu, and A.Y. Cho, "Short wavelength ( $\lambda \sim 3.4 \mu\text{m}$ ) quantum cascade laser based on strained compensated InGaAs/AlInAs," *Appl. Phys. Lett.*, vol. 72, no. 6, pp. 680–682, 1998.
- [3] J. Faist, F. Capasso, C. Sirtori, D.L. Sivco, J.N. Baillargeon, A.L. Hutchinson, S.N.G. Chu, and A.Y. Cho, "High power mid-infrared ( $\lambda \sim 5 \mu\text{m}$ ) quantum cascade lasers operating above room temperature," *Appl. Phys. Lett.*, vol. 68, no. 26, pp. 3680–3682, 1996.
- [4] C. Gmachl, A. Tredicucci, F. Capasso, A.L. Hutchinson, D.L. Sivco, J.N. Baillargeon, and A.Y. Cho, "High-power  $\lambda \approx 8 \mu\text{m}$  quantum cascade lasers with near optimum performance," *Appl. Phys. Lett.*, vol. 72, no. 24, pp. 3130–3132, 1998.
- [5] D. Hofstetter, J. Faist, M. Beck, A. Muller, and U. Oesterle, "Demonstration of high-performance  $10.16 \mu\text{m}$  quantum cascade distributed feedback lasers fabricated without epitaxial regrowth," *Appl. Phys. Lett.*, vol. 75, no. 5, pp. 665–667, 1999.
- [6] C. Gmachl, F. Capasso, A. Tredicucci, D.L. Sivco, A.L. Hutchinson, and A.Y. Cho, "Long wavelength ( $\lambda \simeq 13 \mu\text{m}$ ) quantum cascade lasers," *Electron. Lett.*, vol. 34, no. 11, pp. 1103–1104, 1998.
- [7] A. Tredicucci, C. Gmachl, F. Capasso, D.L. Sivco, A.L. Hutchinson, and A.Y. Cho, "Long wavelength superlattice quantum cascade lasers at  $\lambda \simeq 17 \mu\text{m}$ ," *Appl. Phys. Lett.*, vol. 74, no. 5, pp. 638–640, 1999.
- [8] Capasso F., A. Tredicucci, C. Gmachl, D.L. Sivco, A.L. Hutchinson, A.Y. Cho, and G. Scamarcio, "High-performance superlattice quantum cascade lasers," *IEEE J. Sel. Top. Quant. Elect.*, vol. 5, no. 3, pp. 792–807, 1999.
- [9] A. Tredicucci, F. Capasso, C. Gmachl, D.L. Sivco, A.L. Hutchinson, and A.Y. Cho, "High performance

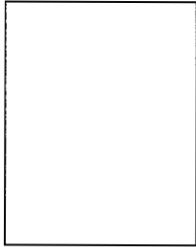
- interminiband quantum cascade lasers with graded superlattices,” *Appl. Phys. Lett.*, vol. 73, no. 15, pp. 2101–2103, 1998.
- [10] D.F. Nelson, R.C. Miller, and D.A. Kleinman, “Band nonparabolicity effects in semiconductor quantum-wells,” *Phys. Rev. B*, vol. 35, no. 14, pp. 7770–7773, 1987.
- [11] R.P. Leavitt, “Empirical 2-band model for quantum-wells and superlattices in an electric-field,” *Phys. Rev. B*, vol. 44, no. 20, pp. 11270–11280, 1991.
- [12] C. Sirtori, F. Capasso, J. Faist, and S. Scandolo, “Nonparabolicity and a sum-rule associated with bound-to-bound and bound-to-continuum intersubband transitions in quantum-wells,” *Phys. Rev. B*, vol. 50, no. 12, pp. 8663–8674, 1994.
- [13] J.N. Schulman, “ $\text{Ga}_{1-x}\text{Al}_x\text{As-Ga}_{1-y}\text{Al}_y\text{As-GaAs}$  double-barrier structures,” *J. Appl. Phys.*, vol. 60, no. 11, pp. 3954–3958, 1986.
- [14] D.Z. Ting, E.T. Yu, D.A. Collins, D.H. Chow, and T.C. McGill, “Modeling of novel heterojunction tunnel structures,” *J. of Vac. Sci. Tech. B*, vol. 8, no. 4, pp. 810–816, 1990.
- [15] G. Bastard, “Theoretical investigations of super-lattice band-structure in the envelope-function approximation,” *Phys. Rev. B*, vol. 25, no. 12, pp. 7584–7597, 1982.
- [16] M.S. Kiledjian, J.N. Schulman, and K.L. Wang, “Absorption in  $\text{GaAs/Ga}_{1-x}\text{Al}_x\text{As}$  quantum-wells with resonant barriers for improved responsivity,” *Phys. Rev. B*, vol. 44, no. 11, pp. 5616–5621, 1991.
- [17] J. Faist, F. Capasso, D.L. Sivco, L. Hutchinson, C. Sirtori, S.N.G. Chu, and A.Y. Cho, “Quantum cascade laser - temperature-dependence of the performance-characteristics and high  $t_0$  operation,” *Appl. Phys. Lett.*, vol. 65, no. 23, pp. 2901–2903, 1994.
- [18] G. Scamarcio, F. Capasso, C. Sirtori, J. Faist, A.L. Hutchinson, D.L. Sivco, and A.Y. Cho, “High-power infrared (8-micrometer wavelength) superlattice lasers,” *Science*, vol. 276, no. 5313, pp. 773–776, 1997.
- [19] M. Helm, “Infrared-spectroscopy and transport of electrons in semiconductor superlattices,” *Semicond. Sci. Tech.*, vol. 10, no. 5, pp. 557–575, 1995.
- [20] A. Tredicucci, F. Capasso, C. Gmachl, D.L. Sivco, A.L. Hutchinson, A.Y. Cho, J. Faist, and G. Scamarcio, “High-power inter-miniband lasing in intrinsic superlattices,” *Appl. Phys. Lett.*, vol. 72, no. 19, pp. 2388–2390, 1998.
- [21] C. Gmachl, F. Capasso, J. Faist, A.L. Hutchinson, A. Tredicucci, D.L. Sivco, J.N. Baillargeon, S.N.G. Chu, and A.Y. Cho, “Continuous-wave and high-power pulsed operation of index-coupled distributed feedback quantum cascade laser at  $\lambda \approx 8.5 \mu\text{m}$ ,” *Appl. Phys. Lett.*, vol. 72, no. 12, pp. 1430–1432, 1998.



**David Z.-Y. Ting** was born in Taipei, Taiwan in 1957. He received the B.S. degree with honors in physics from the California Institute of Technology, Pasadena, in 1980, and the M.S. and Ph.D. degrees in physics from the University of Illinois at Urbana-Champaign in 1981 and 1986, respectively. He was a senior research fellow in the Department of Applied Physics at Caltech before joining the National Tsing Hua University, Hsinchu, Taiwan, as an Associate Professor of Physics in 1995. In 1998 he joined Jet Propulsion Laboratory, Pasadena, CA, and is currently a Senior Member of Engineering Staff in the Device Research and Applications

Section. He is also a Visiting Associate in the Department of Applied Physics at Caltech. His research activities include the theoretical studies of electronic and optical properties of semiconductor alloys, quantum wells, and superlattices, modeling of heterostructure tunnel devices and lasers, quantum transport in nanostructure, and

optical simulations. Results of his research have been reported in over 80 research publications and in many technical presentations. Dr. Ting is a member of the American Physical Society, IEEE Lasers and Electro-Optics Society, and the Materials Research Society.



Martin Young received the MS in Applied Physics from Binghamton University in 1988. From 1988 to 1996 he was a member of technical staff in the Photonic Circuits Research Department at AT&T Bell Labs where he was engaged in research on indium phosphide (InP) based photonic integrated circuits and MOVPE crystal growth. During this time, he developed devices for wavelength division multiplexing (WDM) including laser arrays with integrated modulators, amplifiers, and waveguide combiners. Since 1996 he has been a member of technical staff in the Photonics Technology Group at the Jet Propulsion Laboratory where he continues to work on photonic devices for communications, high power, narrow linewidth lasers for interferometric applications, and tunable diode lasers for absorption spectroscopy.

Fig. 1. Schematic illustration of the two-band tight-binding (sp) model. The on-site energies are given by  $E_s$  and  $E_p$ , and the hopping matrix elements by  $-u$  and  $t$ . The distance between successive unit cells is  $d$ .

Fig. 2. Band diagram of the graded superlattice with computed energy levels and s-component of probability densities.

Fig. 3. Schematic illustration of the alignment of active and injector region states under various biasing conditions.

Fig. 4. Energy levels as functions of applied bias in a single stage of a graded superlattice QCL structure.

Fig. 5. Computed energy levels and the probability densities for states involved in the lasing transition are shown on the band diagram of a graded superlattice biased for lasing. Right panel shows the transmission probability spectrum through the injector.

Fig. 6. Oscillator strengths between the upper lasing state and six states immediately below it are shown as functions of applied bias. The upper panel contains results for a structure with the active superlattice only, while the lower includes the active superlattice and the injector. Results for the lasing transition are indicated by solid lines.

Fig. 7. Sensivity analysis of superlattice QCL structure to uniform scaling. Wavelength, upper lasing state transmission probability through injector, and oscillator strength between lasing states are computed as functions of applied bias; only results in the operating range are shown.

Fig. 8. Sensivity analysis of superlattice QCL structure to the random displacement of interfaces. Each interface of the standard structures is randomly displaced by  $-1, 0, \text{ or } 1 \text{ \AA}$  ( $|\Delta x| = 1 \text{ \AA}$ ), all with equal probability. Results for ten test structures are shown along the with those for the reference structure (in thick solid lines).

Fig. 9. The same as Fig. 8, except larger random displacement value of  $|\Delta x| = 3 \text{ \AA}$  is used. Note the difference in scales from Fig. 8.

Fig. 10. Sensivity analysis of superlattice QCL structure to interface grading. Results for structurew with ramp widths of  $10 \text{ \AA}$  and  $6 \text{ \AA}$  are compared to those from a structure with sharp interfaces.

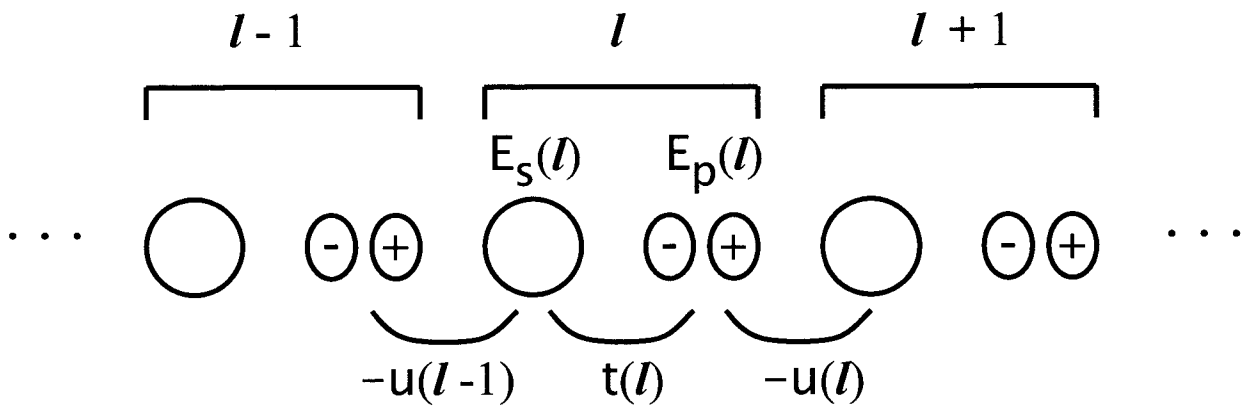


Figure 1, Ting and Young

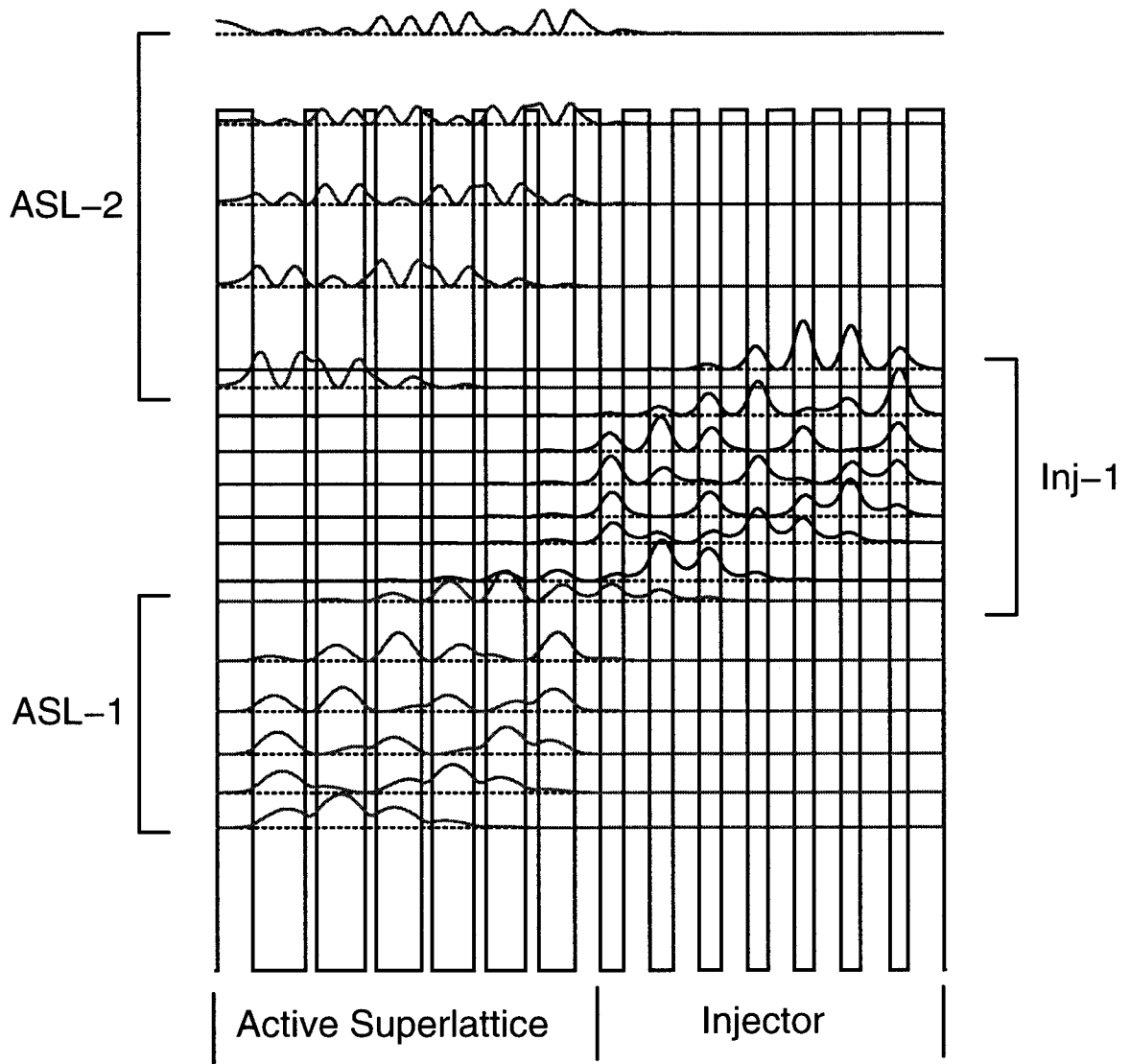


Figure 2, Ting and Young

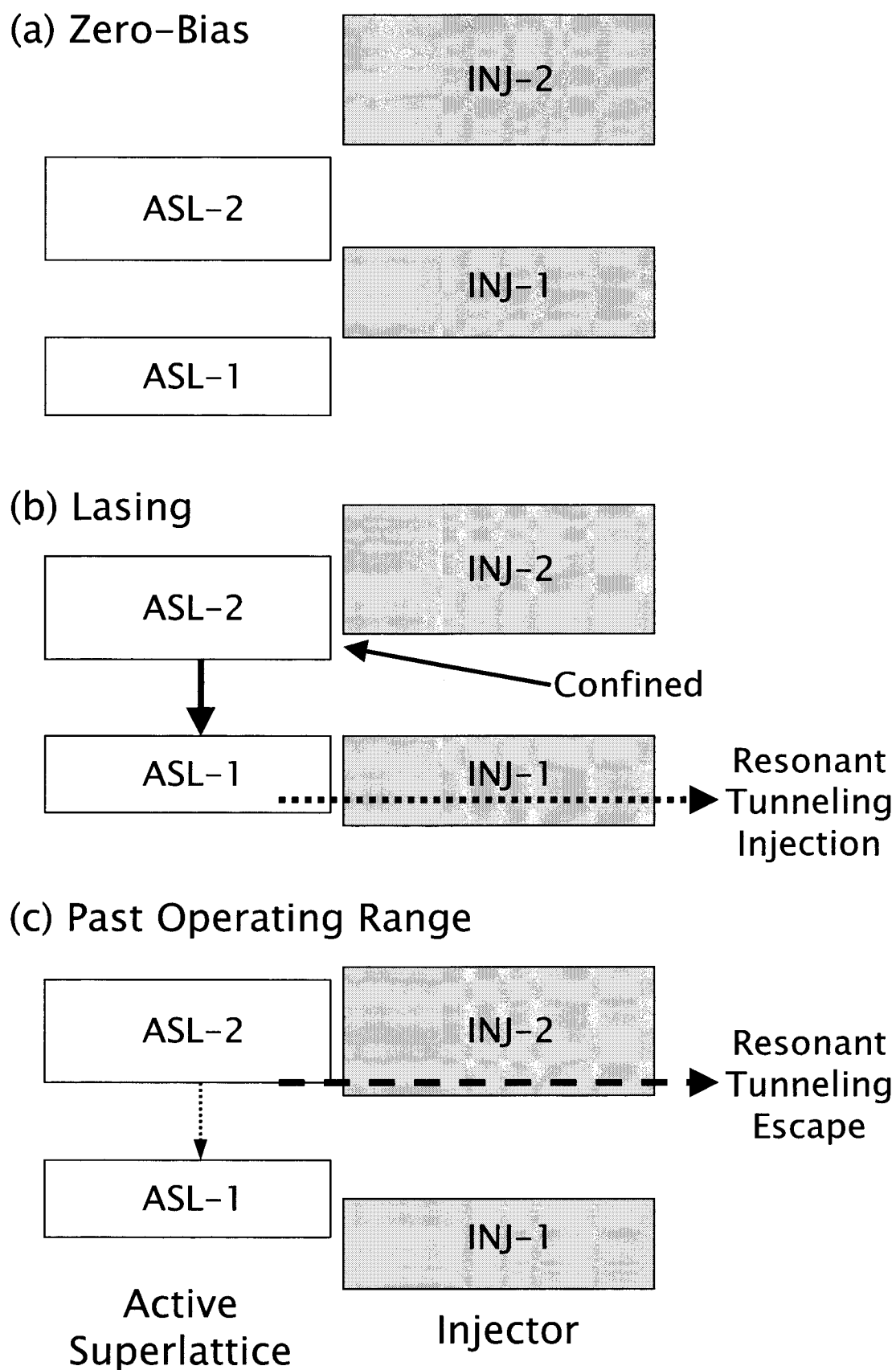


Figure 3, Ting and Young

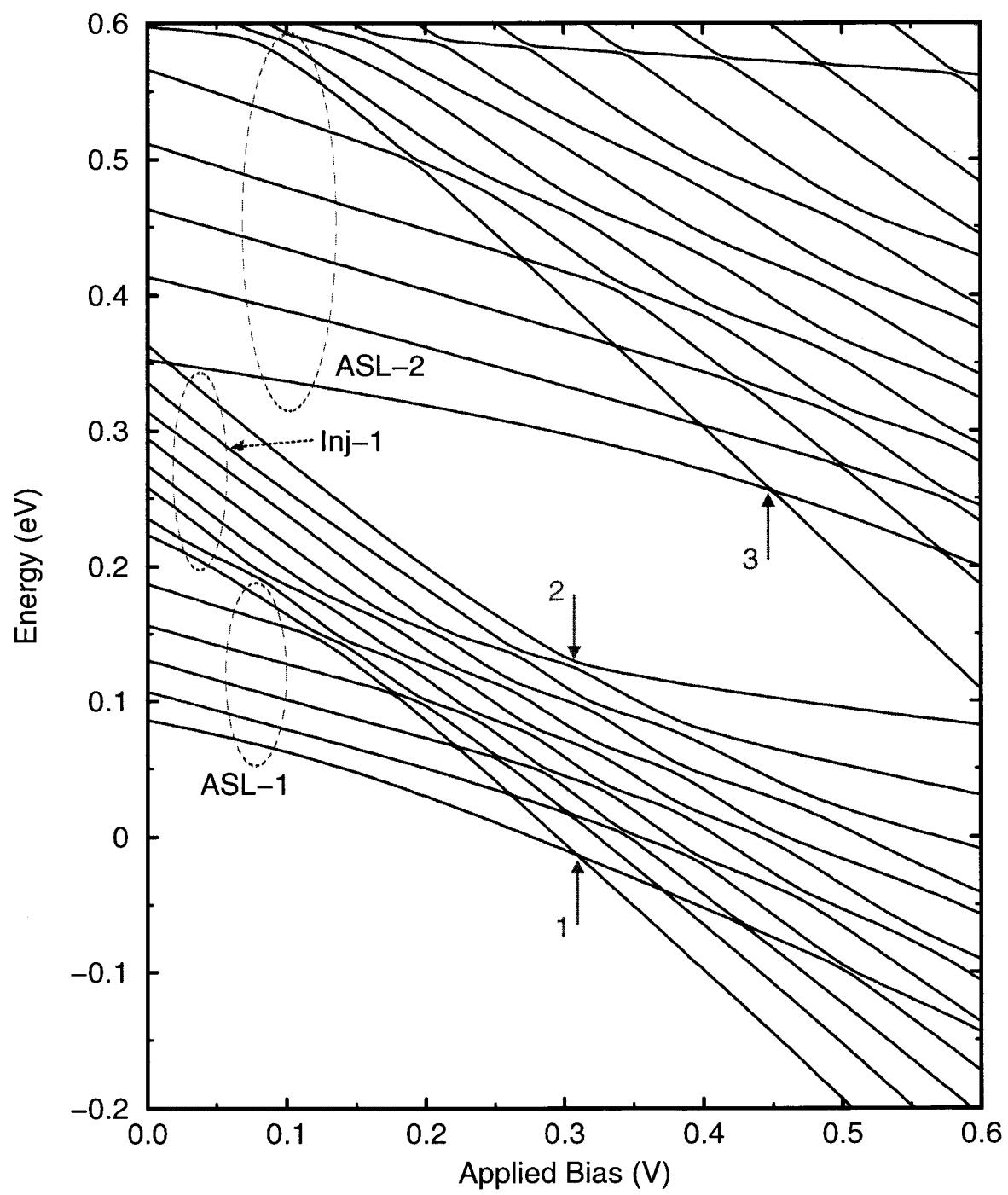


Figure 4, Ting and Young

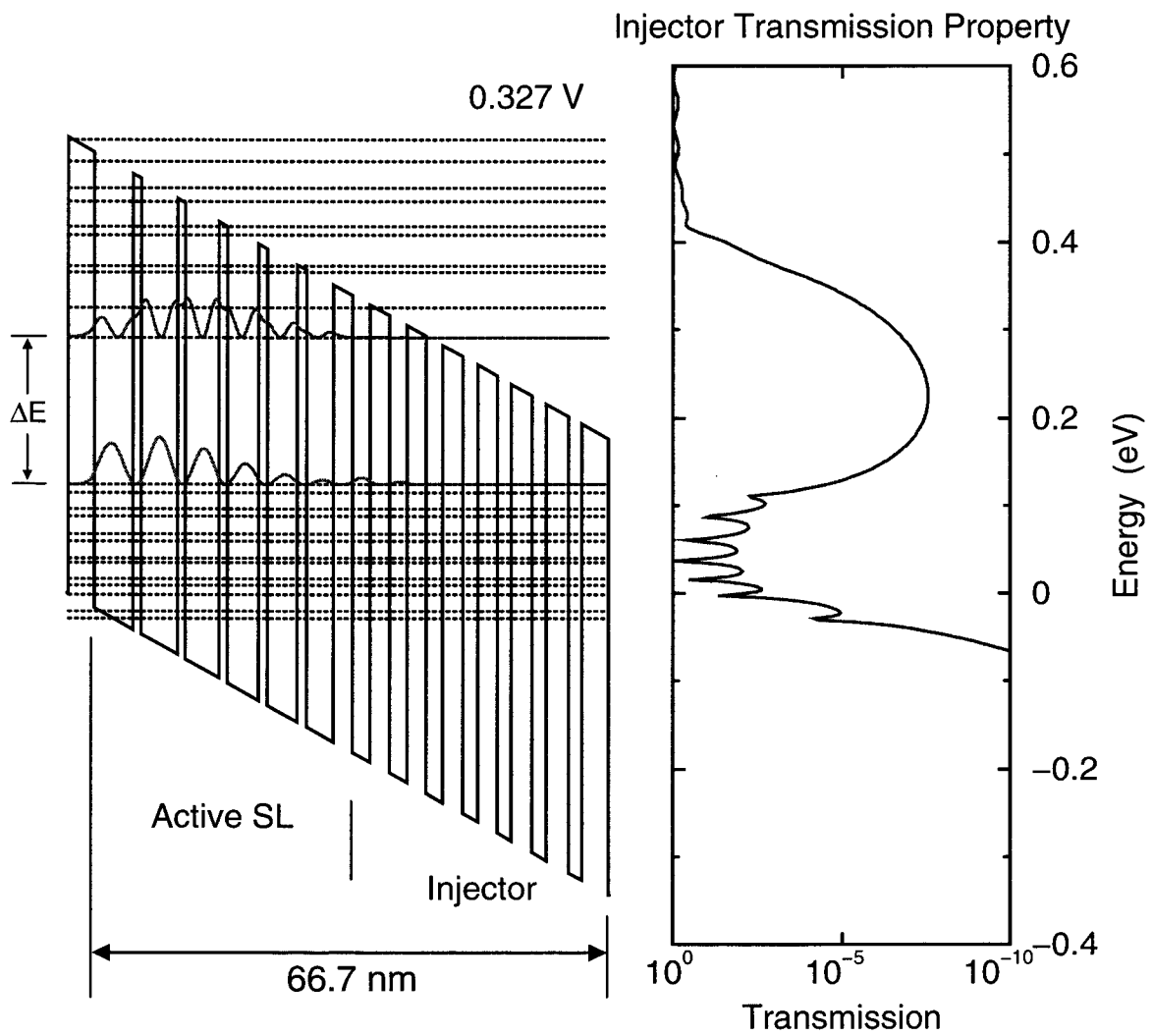


Figure 5, Ting and Young

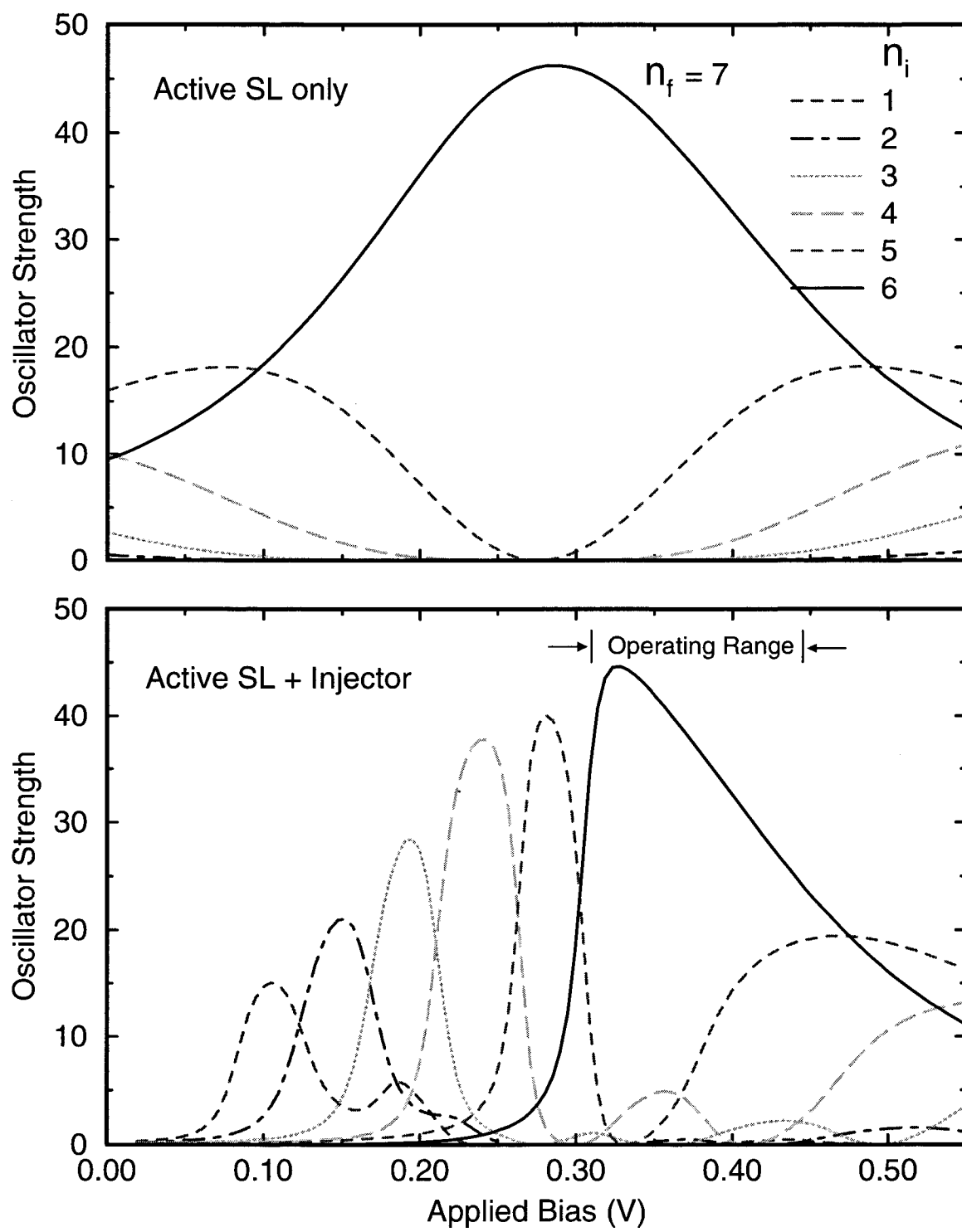


Figure 6, Ting and Young

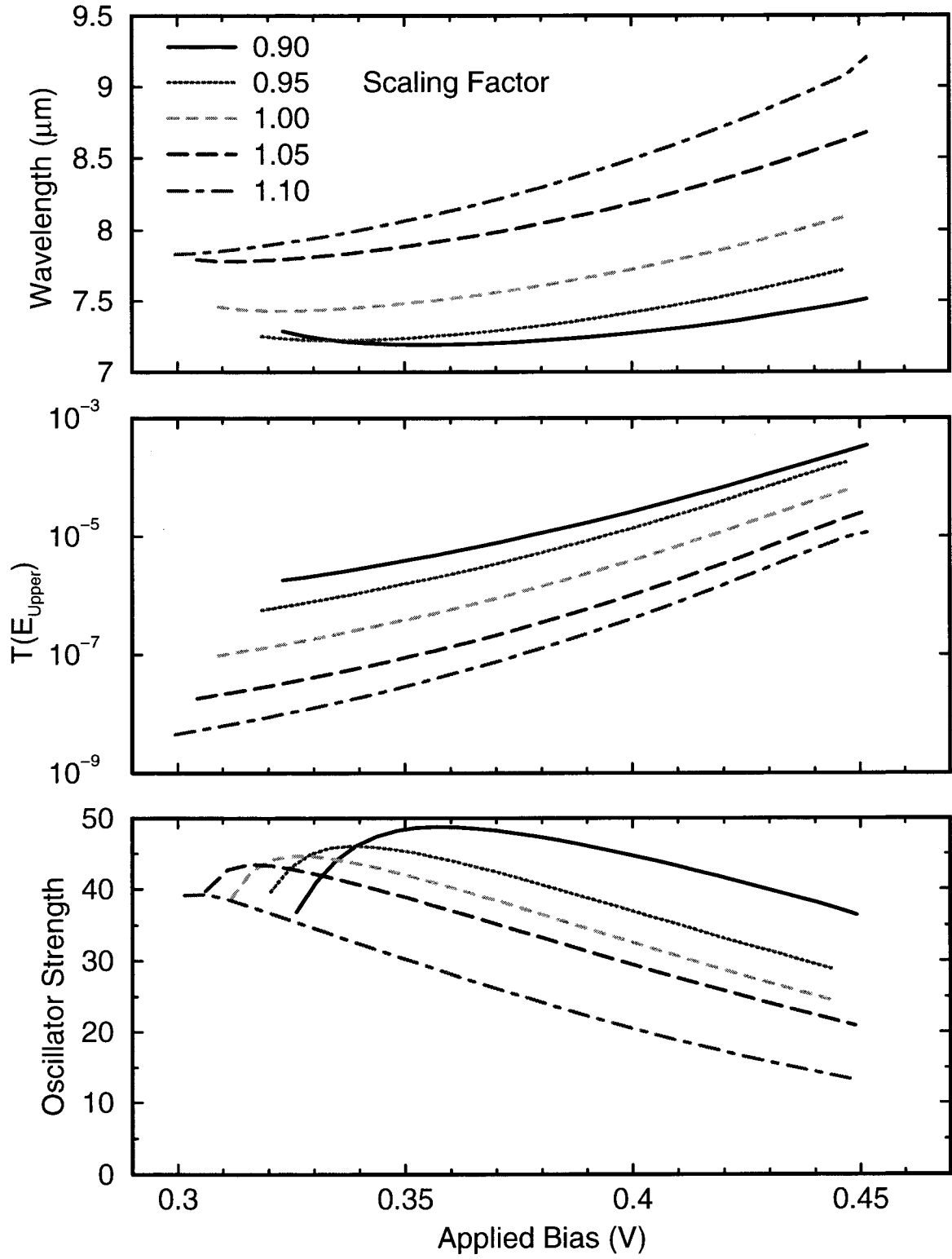


Figure 7, Ting and Young

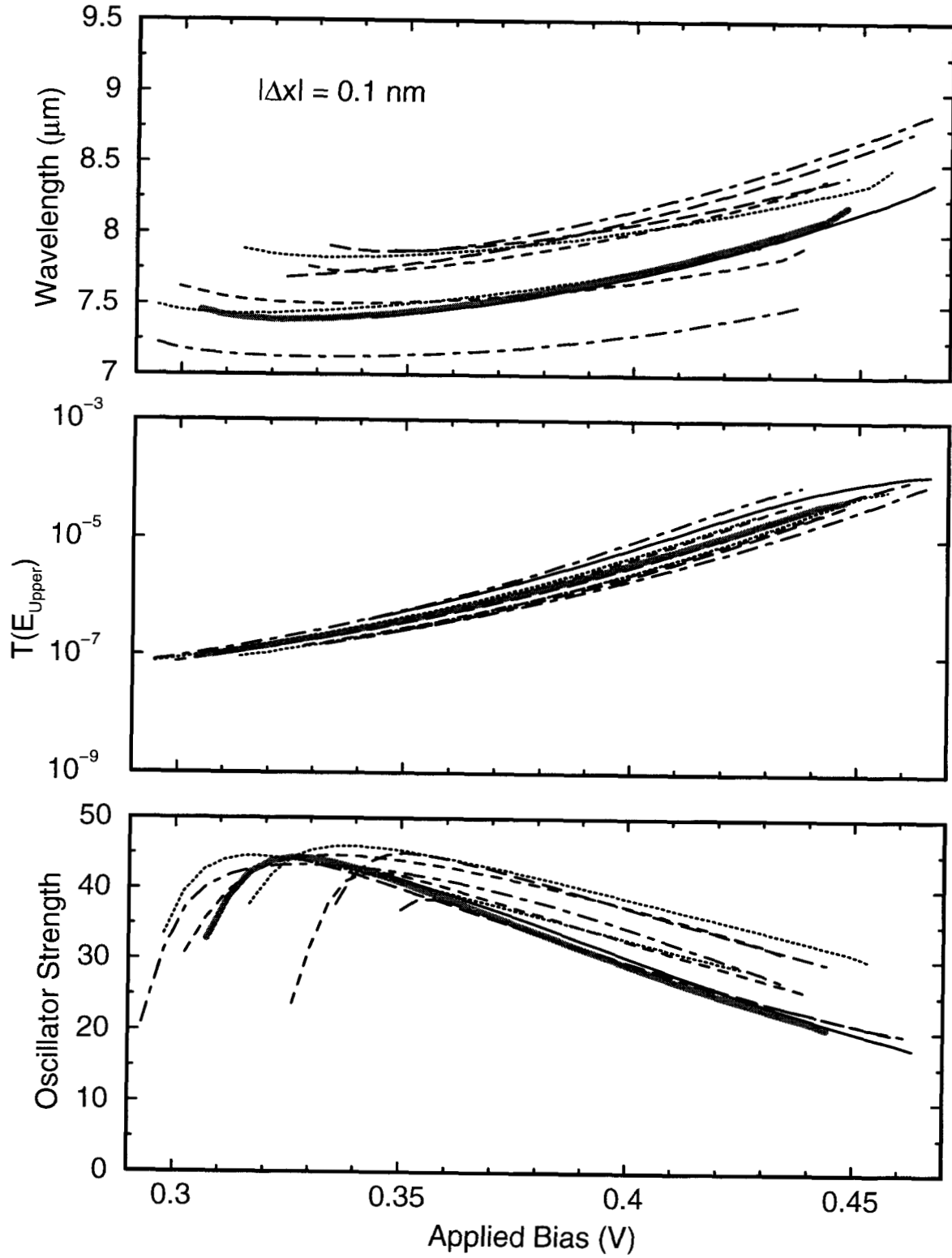


Figure 8, Ting and Young

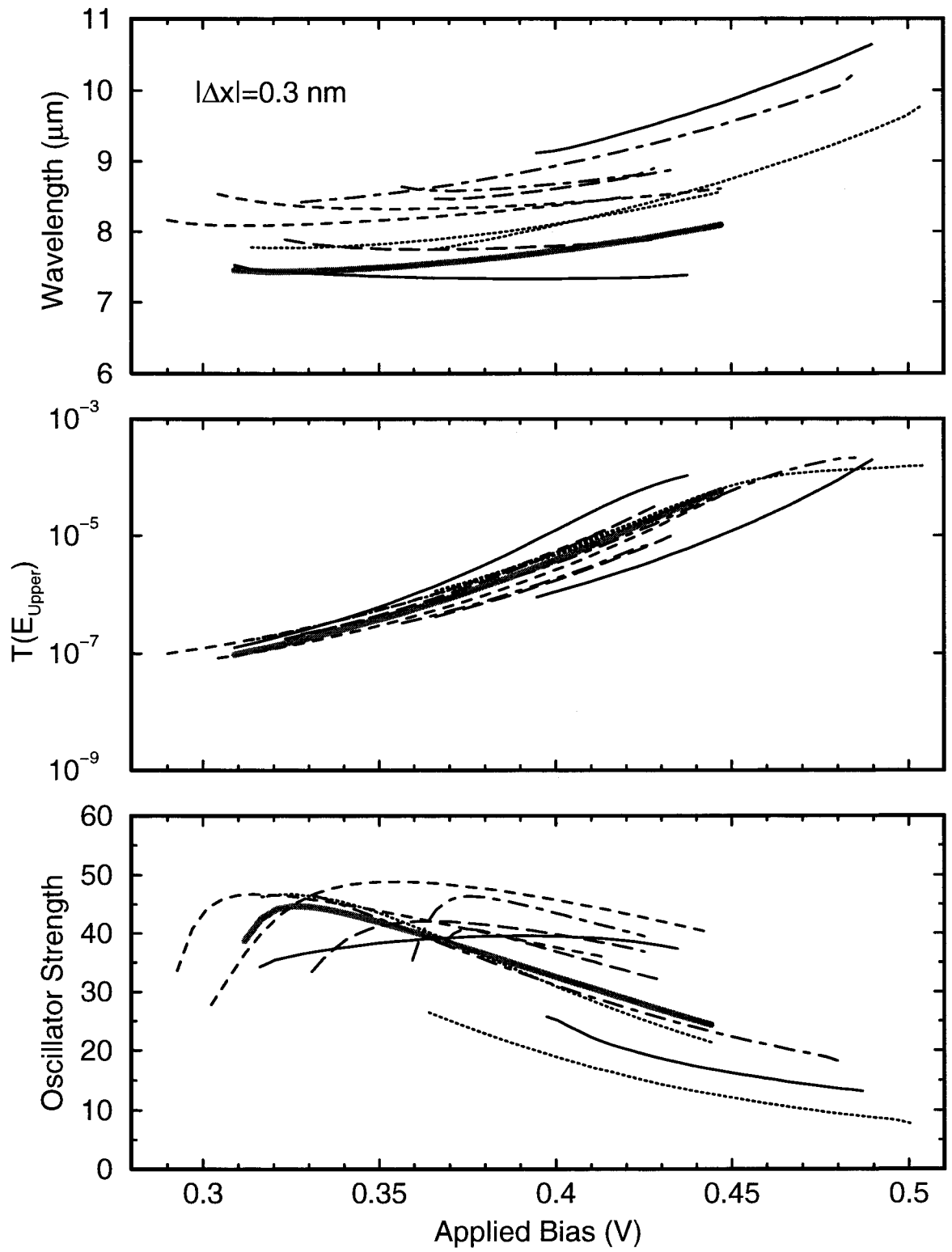


Figure 9, Ting and Young

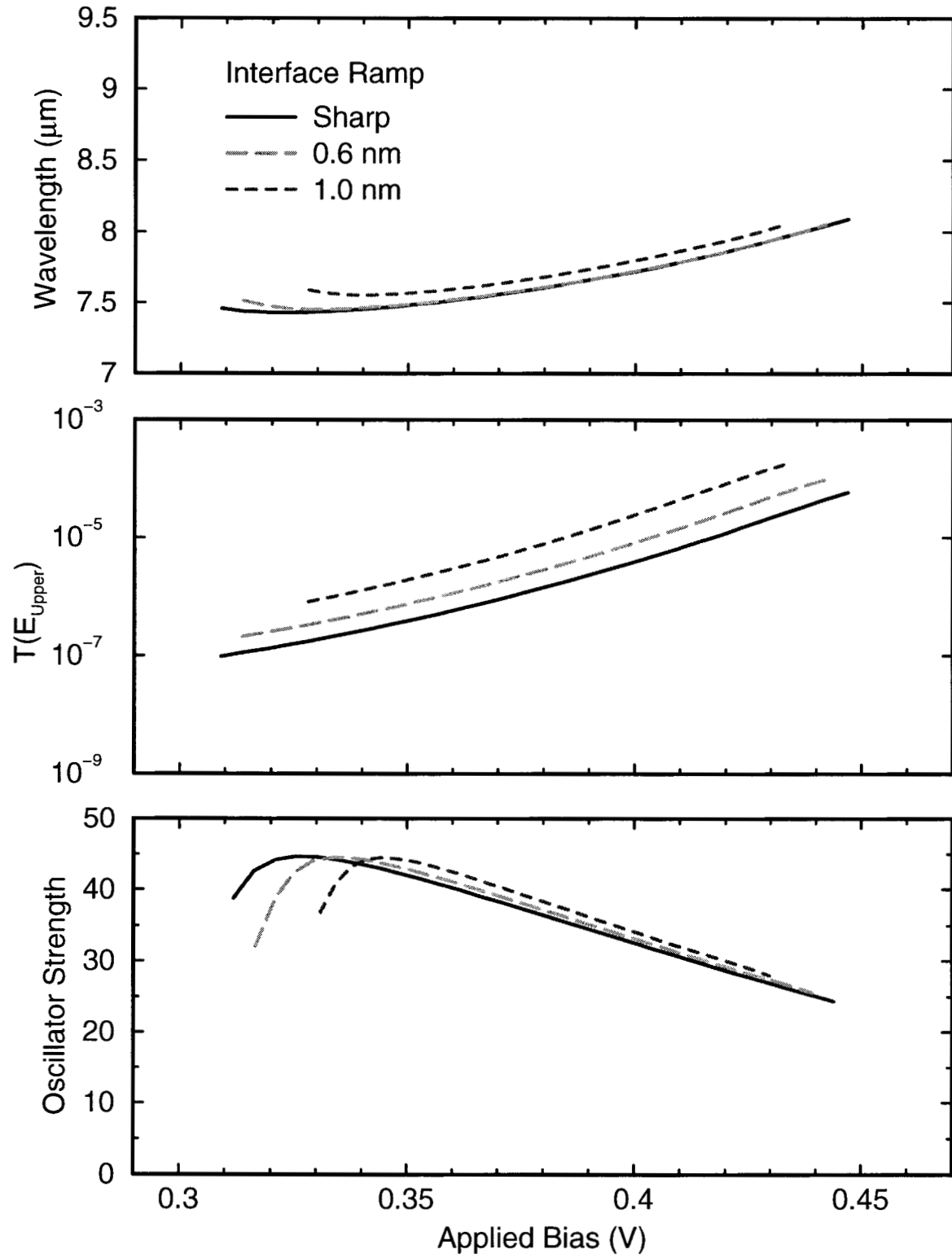


Figure 10, Ting and Young